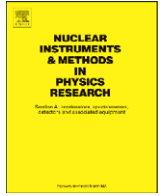




Contents lists available at ScienceDirect

# Nuclear Instruments and Methods in Physics Research A

journal homepage: [www.elsevier.com/locate/nima](http://www.elsevier.com/locate/nima)

## Advances in multipixel Geiger-mode avalanche photodiodes (silicon photomultipliers)

Yuri Musienko <sup>a,b,\*</sup><sup>a</sup> Department of Physics, Northeastern University, Boston, MA 02115, USA<sup>b</sup> Institute for Nuclear Research RAS, pr. 60-letiya Oktyabrya 7a, 117312 Moscow, Russia

### ARTICLE INFO

Available online 19 August 2008

#### Keywords:

Silicon avalanche photodiodes  
Silicon photomultiplier  
Light detection  
Photon counting

### ABSTRACT

We review the current status of developments in multipixel Geiger-mode avalanche photodiodes (also referred to as SiPMs, SSPMs, MRS APDs, AMPDs, MPPCs) and discuss their advantages and limitations for high-energy physics applications.

© 2008 Elsevier B.V. All rights reserved.

### 1. Introduction

One of the most promising techniques to detect single photons is using an avalanche photodiode (APD) operated in Geiger mode. In this mode, an APD is biased above the breakdown voltage with the breakdown occurring only when initiated by a thermal- or photo-generated primary electron. Thus every primary electron which initiates a breakdown pulse can be detected. After the discharge is quenched, using passive or active quenching circuit, the voltage can be reset with a short dead time to await the next electron. First Geiger-mode APDs (G-APD) were developed and studied for photon detection in the early 1960s [1–3]. Since then, significant progress was made in the development of APDs operated in Geiger mode. A remarkably high (>50%) photon detection efficiency for a wide range of wavelengths (540–850 nm) was measured with a small (200 μm diameter) reach-through G-APD [4]. Excellent single-photon timing resolution of ~35 ps (FWHM) has been measured using a 100-μm-diameter planar G-APD [5].

The disadvantages of single-pixel G-APDs, which limit their application to SciFi trackers and HEP calorimetry, are small APD-active area and their lack of a proportional response to multiphoton events. The maximum active size for state-of-the-art single-pixel G-APDs is limited to 0.5 mm diameter. Devices with a few square millimeters active area cannot operate properly at room temperature. They can be blocked by a high dark-noise generation rate ( $10^5$ – $10^6$  counts/mm<sup>2</sup>) due to the relatively long reset time (typically several microseconds) following a Geiger discharge for an APD operated with passive quenching circuit

(PQC). This time is defined by the values of the APD capacitance (>10 pF/mm<sup>2</sup>) and the quenching resistor, which should be higher than 100 kΩ to be able to quench an avalanche. The APD dead time can be reduced by using an active quenching circuit (AQC). Dead times as low as 36 ns were demonstrated by Ghioni et al. [6] using a specially designed AQC.

Proportional response to multiphoton events becomes possible in a design where many (100–100,000) identical, small-area APDs (pixels or cells) are placed on a common substrate and electrically connected in parallel [7,8]. The first multipixel G-APDs were developed in the USSR at the end of the 1980s [9]. They were designed to be sensitive to red light and had rather low quantum efficiency (<1%) in the blue-green part of the visible spectrum. Since then, the performance of G-APDs for the detection of blue-green photons has been greatly improved [10,11], causing significant interest for these devices both in the scientific and industrial communities. Indeed, properties of these APDs such as high gain and quantum efficiency (which potentially can reach that of silicon photodiodes), low noise, non-sensitivity to ionizing radiation and magnetic fields, compactness, robustness and anticipated low production costs at large volumes makes them very attractive candidates for many applications.

### 2. Photon detection efficiency

At room temperature, the dependence of G-APD photon detection efficiency on the bias voltage  $U$ , wavelength of light  $\lambda$  and temperature  $T$  can be expressed by the following equation:

$$PDE(\lambda, U, T) = QE(\lambda) \times G_F \times P_B(\lambda, U, T) \quad (1)$$

where  $QE(\lambda)$  is the quantum efficiency of the G-APD single cell measured at unity gain and wavelength  $\lambda$ ,  $G_F$  is the ratio of the

\* Corresponding author at: Department of Physics, Northeastern University, Boston, MA 02115, USA. Tel.: +41 22 767 16 31; fax: +41 22 767 89 30.

E-mail address: [louri.Musienko@cern.ch](mailto:louri.Musienko@cern.ch)

light-sensitive area to the total G-APD area (geometric factor), and  $P_B(\lambda, U, T)$  is the wavelength-, temperature- and voltage-dependent probability that a primary photoelectron (or hole) triggers the cell breakdown.

Most G-APDs currently produced by CPTA/Photonique [12], SensL [13], FBK-irst [14], MEPHl/PULSAR [15] are based on the  $n^+p\text{-}\pi\text{-}p^+$  or  $n^+p\text{-}p^+$  (p-type) structure with thicknesses of the depleted regions (regions  $p$  and  $\pi$ ) ranging from 3 to  $10\ \mu\text{m}$  and the depths of the  $n^+p$  junctions ranging from 0.3 to  $1\ \mu\text{m}$  (see, for example, Ref. [17]). This structure is optimal for green-red light detection ( $1\text{--}3\ \mu\text{m}$  absorption depth in silicon). Blue/UV light ( $400\text{--}450\ \text{nm}$ ) has a small absorption depth in silicon ( $100\text{--}500\ \text{nm}$ ) and most of it is absorbed very close to the surface of the G-APD cell, inside the  $n^+p$  junction. Most photo-carriers (electrons and holes) created by light in the non-depleted  $n^+$  layer recombine and do not produce electrical signals. Photo-carriers produced by blue/UV light in the  $p$  region have low probability to cause pixel breakdown. The electrons created close to the G-APD surface cross only a small part of the high-electric-field region and do not trigger an avalanche. In silicon, holes have a smaller ionization coefficient than electrons and subsequently have a smaller probability to cause an avalanche [18].

For most HEP applications, G-APDs with high sensitivity to blue/green light are required. Fig. 1 shows the spectral responses of the newly developed  $1\ \text{mm}^2$  area CPTA/Photonique ( $43\ \mu\text{m}$  pixel pitch) [19] and FBK-irst ( $50\ \mu\text{m}$  pixel pitch) [20] G-APDs measured at room temperature and operated at maximum bias voltage (further increasing of the bias voltage will cause excessive noise and/or instability of G-APD operation). To improve G-APD sensitivity in the blue/UV part of the spectrum, the thicknesses of the  $n^+$  and  $p$  layers in these devices are reduced (in the FBK-irst G-APDs they are  $0.1$  and  $0.6\ \mu\text{m}$ , respectively [21]) and geometric factors are increased up to  $\sim 70\%$  for CPTA/Photonique and  $\sim 50\%$  FBK-irst G-APDs. Details on the measurement techniques used to characterize these devices can be found in Ref. [22].

Significantly higher photon detection efficiency for UV/blue light is achieved with G-APDs based on  $p^+p\text{-}n^+$  (n-type) structure. The high-electric-field region in this APD (defined by the  $p\text{-}n^+$  junction) is “buried” at a depth of  $1\text{--}3\ \mu\text{m}$ . Electrons which are created in front of the  $p\text{-}n^+$  junction by blue/UV light enter the high-electric-field region and initiate an avalanche breakdown. The probability of Geiger discharge due to electrons is high even at low over-voltages. Primary holes move in the direction of the  $p^+$  electrode and do not initiate the avalanche.

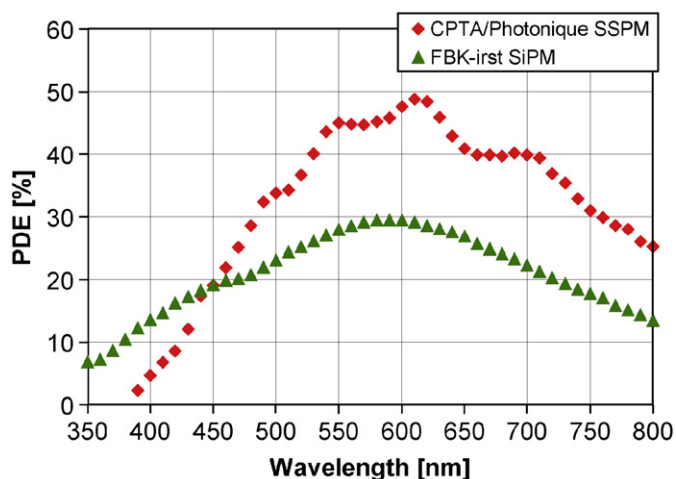


Fig. 1. Photon detection efficiency as a function of the wavelength of light for p-type CPTA/Photonique ( $U = 42\ \text{V}$ ) and FBK-irst ( $U = 35.5\ \text{V}$ ) G-APDs, measured at room temperature.

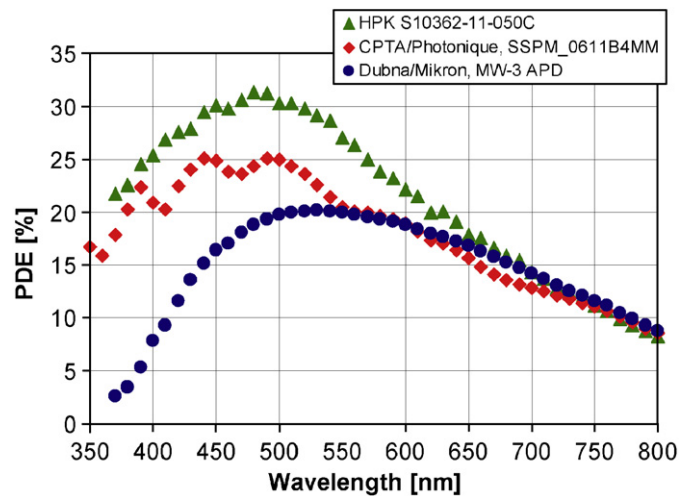


Fig. 2. Photon detection efficiency as a function of the wavelength of light for n-type Hamamatsu ( $U = 70.3\ \text{V}$ ), CPTA/Photonique ( $U = 36\ \text{V}$ ) and Dubna/Mikron ( $U = 119.6\ \text{V}$ ) G-APDs, measured at room temperature.

In addition, the  $p^+$  layer can be made very thin ( $< 100\ \text{nm}$ ), reducing losses due to recombination of photo-carriers in this non-depleted layer. Fig. 2 shows the dependence of photon detection efficiency of the three n-type G-APDs measured at room temperature for highest possible bias. One observes significant improvement in G-APD sensitivity for blue light. For Hamamatsu and CPTA/Photonique G-APDs, PDE reaches  $25\text{--}30\%$  for  $450\ \text{nm}$  light.

### 3. Dark counts and after-pulsing

The main source of noise limiting the G-APD performance is the dark count rate. It is composed of the primary pulses triggered by carriers thermally generated in the depleted region and after-pulses caused by trapped carriers and their subsequent release. Typical G-APD dark count rates at room temperature are in the range of several hundred kHz to several MHz per square millimeter sensor area.

Fig. 3 shows the distribution of time intervals between dark pulses for n-type Hamamatsu and p-type CPTA/Photonique G-APDs measured at  $70.3$  and  $37.9\ \text{V}$  bias, respectively. The dark count rate of  $366\ \text{kHz}$  for Hamamatsu and  $1.95\ \text{MHz}$  for CPTA/Photonique G-APDs were measured at a threshold corresponding to  $0.5$  photoelectron signal. The time distribution of the primary dark pulses should follow a Poisson distribution. This is true for both devices in the range of long (more than  $1\ \mu\text{s}$ ) time intervals. However, for short time intervals (i.e.  $< 500\ \text{ns}$  for Hamamatsu and  $< 40\ \text{ns}$  for CPTA/Photonique G-APDs), the deviation from a Poisson distribution is clearly visible. Using this data, the probability that primary dark pulses trigger an after-pulse was calculated for both G-APDs. It was found to be  $\sim 20\%$  for Hamamatsu and  $\sim 3\%$  for CPTA/Photonique G-APDs.

### 4. Optical cross-talk

We observe that an increase in the G-APD signal threshold leads to a slower drop in the dark count rate as expected from simple random coincidences. This discrepancy is linked to optical cross-talk between the G-APD pixels where the light emitted during the avalanche breakdown in one cell can trigger a breakdown in a neighbouring cell [23]. This optical cross-talk

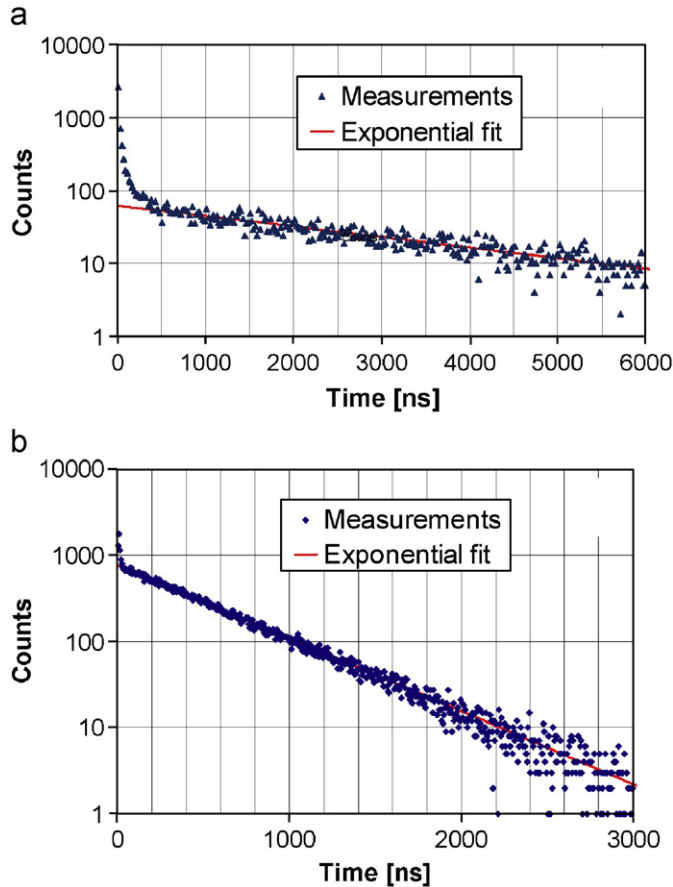


Fig. 3. Distribution of time intervals between dark count pulses for n-type Hamamatsu at  $U = 70.3\text{ V}$  (a) and p-type CPTA/Photonique at  $U = 37.9\text{ V}$  (b) G-APDs.

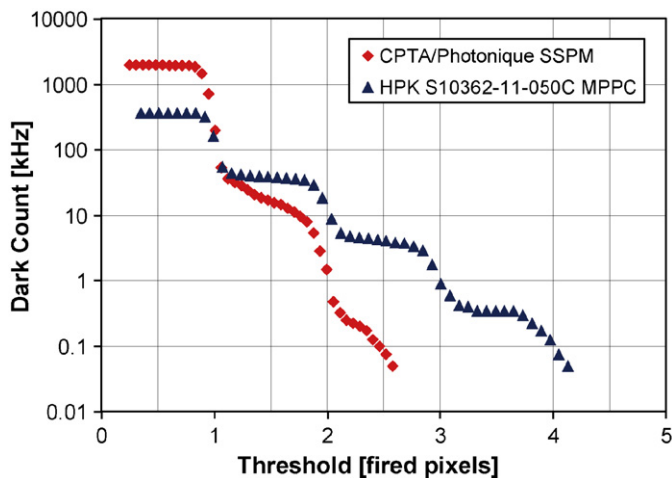


Fig. 4. Dark count rates as a function of an electronics threshold for p-type CPTA/Photonique ( $U = 37.9\text{ V}$ ) and n-type Hamamatsu ( $U = 70.3\text{ V}$ ) G-APDs.

imposes a lower limit on the G-APD geometric factor as individual cells cannot be placed arbitrarily close to one another.

To reduce the effect of optical cross-talk, CPTA first introduced trenches to separate neighbouring cells [24]. Fig. 4 shows the dependence of dark count rate for CPTA/Photonique (with trenches) and Hamamatsu [16] G-APD (without trenches) as a function of the electronics threshold measured at room temperature. Using trenches, the optical cross-talk of CPTA/Photonique

G-APDs was reduced to  $<1\%$ . For Hamamatsu G-APD, where optical cell separation does not use the trench technology, optical cross-talk was measured to be  $\sim 10\%$ . It is worth mentioning that both devices operated at a bias voltage corresponding to a PDE of 30% at 515 nm.

## 5. Excess noise factor

Due to after-pulsing and optical cross-talk between cells, the multiplication noise of G-APDs is not negligible despite the fact that individual cells exhibit very small signal spread. In analogy to PMTs and APDs, multiplication noise can be expressed in terms of an “excess noise factor”,  $F$  (see, for example, Ref. [22]). G-APD excess noise factor can be measured from the width of single electron spectra and calculated using

$$F = 1 + \frac{\sigma^2}{M^2} \quad (2)$$

where  $M$  is the G-APD gain and  $\sigma^2$  is its variance. For example, excess noise factor of 1.05 was measured for CPTA/Photonique G-APD at 37.9 V and 1.3 was measured for Hamamatsu device at 70.3 V.

## 6. Temperature sensitivity

G-APD signal stability depends mainly on the stability of the applied bias and the temperature. To describe the dependence of G-APD response on the temperature, one can introduce a temperature coefficient  $k_T$  as follows (see, for example, Ref. [25]):

$$k_T(V) = \frac{1}{A} \times \frac{dA}{dT} \times 100\% \quad (3)$$

where  $A$  is the G-APD signal amplitude and  $T$  is the device temperature.

To find the temperature coefficients for Hamamatsu and CPTA/Photonique G-APDs, the amplitude of the signals from a green LED were measured as a function of the bias at two different temperatures [25] and  $k_T$  was calculated using Eq. (3). The results are shown in Fig. 5. Low temperature sensitivity of CPTA/Photonique G-APD is mainly due to the very high over-voltage  $(V-V_B)/V_B > 0.3$  which can be applied to this APD even at room temperature.

## 7. Timing

The G-APD-active pixel area and thickness of the depleted region are very small. This results in a very fast (few tens of picoseconds) avalanche build-up, and hence a fast response to a photoelectron. Excellent timing resolution ( $\sim 100\text{ ps}$  FWHM) was measured with FBK-irst and CPTA/Photonique G-APDs using single photons [26].

## 8. Active area and dynamic range

HEP calorimetry applications require photosensors with high dynamic range and large area. G-APDs with up to  $3 \times 3\text{ mm}^2$  sensitive area and  $1000\text{ pixel/mm}^2$  cell density are commercially available from Hamamatsu and CPTA/Photonique. Experimental samples with  $5 \times 5\text{ mm}^2$  area are produced by MEPhi/Pulsar [27]. G-APDs with  $3 \times 3\text{ mm}^2$  area and very high pixel density ( $\sim 10,000\text{ pixel/mm}^2$ ) were developed and produced by the Dubna/Mikron APD group [28].

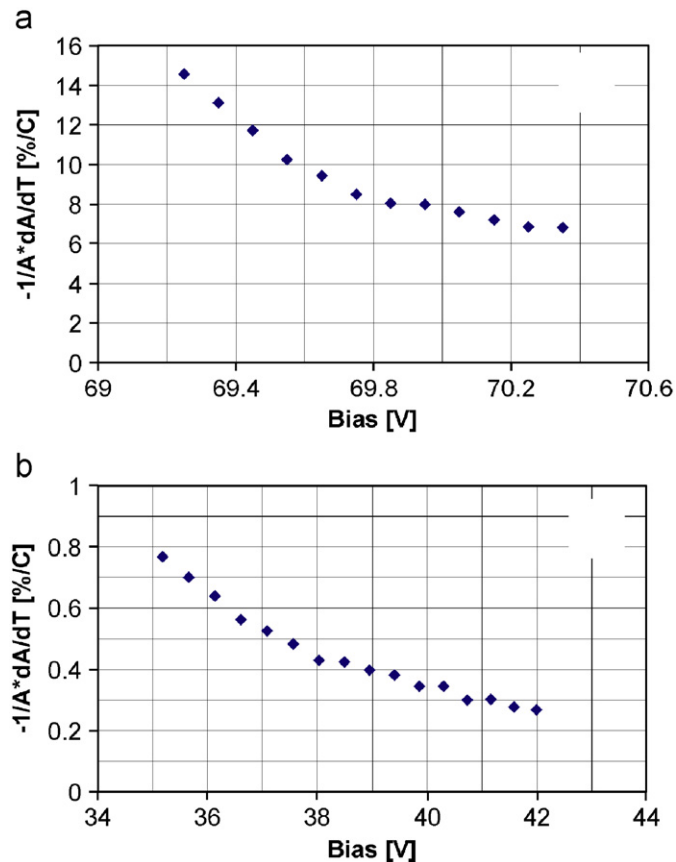


Fig. 5. Temperature coefficients of n-type Hamamatsu (a) and p-type CPTA/Photonique (b) G-APDs in dependence on bias voltage ( $T = 22$  °C).

## 9. Radiation hardness

The radiation hardness of G-APDs was studied using 200 MeV protons [29] and 28 MeV positrons [30]. Significant increases in the G-APD dark current and dark count rates were observed after only  $8 \times 10^{10}$  positrons/cm<sup>2</sup> (equivalent to  $2.7 \times 10^9$  1 MeV n/cm<sup>2</sup>). The change of gain and photon detection efficiency as a function of voltage was found to be small (<15%). Dark currents also increased significantly after irradiation with 200 MeV protons;

however, the tested G-APDs remained operational even after  $10^{11}$  proton/cm<sup>2</sup>.

## 10. Summary

Significant progress has been achieved in the development of G-APDs during the last 2–3 years. Devices with large active area (up to  $5 \times 5$  mm<sup>2</sup>), high photon detection efficiency (30–40% for blue/green light), low optical cross-talk (<1%), fast timing ( $\sim 100$  ps FWHM for single photons) and small temperature coefficient (<0.3%/°C) are now available. All this, and improved understanding of radiation hardness issues, makes these devices excellent candidates for applications in the current and forthcoming HEP experiments.

## References

- [1] R.J. McIntyre, J. Appl. Phys. 32 (6) (1961) 983.
- [2] A. Goetzberger, et al., J. Appl. Phys. 34 (6) (1963) 1591.
- [3] R.H. Haitz, et al., J. Appl. Phys. 35 (5) (1965) 1370.
- [4] H. Dautet, et al., J. Appl. Opt. 32 (21) (1993) 3894.
- [5] A. Gulinatti, et al., Electron. Lett. 41 (5) (2005) 272.
- [6] M. Ghioni, et al., Rev. Sci. Instrum. 67 (1996) 3440.
- [7] V. Golovin, Z. Sadygov, M. Tarasov, N. Yusipov, patent #1644708 of Russia, priority from 1989.
- [8] G. Gasanov, V. Golovin, Z. Sadygov, N. Yusipov, patent #1702831 of Russia, priority from 1989.
- [9] G. Gasanov, V. Golovin, Z. Sadygov, N. Yusipov, Lett. J. Techn. Phys. 16 (1990) 14.
- [10] Y. Musienko, et al., Nucl. Instr. and Meth. A 571 (2006) 362.
- [11] I. Britvitch, Y. Musienko, D. Renker, Nucl. Instr. and Meth. A 567 (2006) 276.
- [12] <http://photonique.ch>.
- [13] <http://www.sensl.com>.
- [14] <http://sipm.itc.it/>.
- [15] <http://pc3k40.exp.mephi.ru/>.
- [16] <http://www.hamamatsu.com>.
- [17] P. Buzhan, et al., ICFA Instrum. Bull. 23 (2001) 28.
- [18] W.G. Oldham, et al., IEEE Trans. Electron. Dev. ED-19 (9) (1972) 1056.
- [19] New development based on SSPM\_0107\_BG type <<http://photonique.ch>>.
- [20] Fondazione Bruno Kessler, Trento, Italy.
- [21] C. Piemonte, et al., IEEE Trans. Nucl. Sci. NS-54 (1982) 236.
- [22] Y. Musienko, S. Reucroft, J. Swain, Nucl. Instr. and Meth. A 567 (2006) 57.
- [23] A. Lacaita, et al., IEEE Trans. Electron. Dev. ED-40 (3) (1993) 577.
- [24] A. Akindinov, et al., Proceedings of the Eighth ICATPP Conference on Advanced Technology and Particle Physics, Villa Erba, Como, 6–10 October 2003, World Scientific, Singapore, 2004.
- [25] Y. Musienko, S. Reucroft, J. Swain, PoS (PD07) 012; <<http://pos.sissa.it/>>.
- [26] G. Collazuol, et al., Nucl. Instr. and Meth. A 581 (2007) 461.
- [27] P. Buzhan, et al., Nucl. Instr. and Meth. A 567 (2006) 78.
- [28] Z. Sadygov, et al., Nucl. Instr. and Meth. A 567 (2006) 70.
- [29] M. Danilov, Nucl. Instr. and Meth. A 581 (2007) 451.
- [30] Y. Musienko, et al., Nucl. Instr. and Meth. A 581 (2007) 433.